

## Flow around a Circular Cylinder with Radial Disturbances at a Low Reynolds Number

*Liming Lin, Xingfu Zhong and Yingxiang Wu*  
Institute of Mechanics, Chinese Academy of Sciences  
Beijing, China

### ABSTRACT

Based on the idea of geometric disturbance in suppressing vortex-induced vibration (VIV), numerical simulations are carried out for a flow past a fixed circular cylinder with different wavy disturbances. Two kinds of disturbances, harmony and cone, are considered. Different wavelengths and wave heights are investigated at a Reynolds number of 100. The introduction of disturbance would increase the drag but reduce the lift for most cases. The local minimum of fluid forces exists, presently, at the non-dimensional wavelength of 6. The typical Kármán vortex is gradually disturbed with the increasing strength of disturbance. Different flow patterns are identified and discussed, such as  $\Omega$ -type vortex and the complete suppression of vortex shedding. Characteristics of effect of disturbance on the generation and distribution of surface vorticity are presented in detail.

**KEY WORDS:** Radial disturbance; circular cylinder; vortex-induced vibration; suppression; riser.

### INTRODUCTION

There are a great number of bluff bodies applied in engineering applications, such as higher buildings in architectures, marine risers or flexible pipelines in subsea oil production. The unsteady wake, associated vortex shedding behind body, results in the fluctuating fluid force. As the frequency of vortex shedding is close to the natural frequency of the body, the synchronization is occurred. The fluid force and oscillating amplitude of body would be suddenly magnified. Such phenomenon is called as the vortex-induced vibration. It has the potential to destroy the structural integrity due to the fatigue damage, even the safety of people and production. In a half century, many researches have been published in understanding the dynamics of VIV. Comprehensive reviews can be referenced in Sarpkaya (1979), Sarpkaya & Isaacson (1981), Sarpkaya (2004), Williamson & Govardhan (2004; 2008), and Gabbai & Benaroya (2005).

Subsequently, many methods have been proposed over recent years to control the wake vortex dynamics for the sake of weakening the vortex shedding, even totally suppressed, as well as the amplitude of the fluid

force. Most of them, as a kind of passive control, are based on disturbing the flow. Earlier, a spiraling arrangement of surface control bumps was proposed by Owen *et al.* (2001). Drag reduction reaches up to 47%. The regular vortex shedding can no longer be detected at certain wave steepness, defined by the ratio of the wave height to the wavelength. It is effective mainly in the great mass-damping parameter. Control rods with equal space around cylinder, investigated by Song *et al.* (2009), can also reduce the transverse response of risers. However, its effectiveness is easy subjected to the marine organism. So far, streamline fairing (Lee & Allen, 2005) exhibits very good aerodynamic performance due to its streamlined shape resulting in the streamlined body shape and the delay of the flow separation. Furthermore, splitter plates can also effectively delay interactions between upper and lower free shear layers, as well as the formation of vortex shedding. To accommodate variable direction of ocean flow, the rotatable equipment is installed on streamline fairing and splitter plates, which could introduce a new problem of dynamical instability. Helical strake (Trim *et al.*, 2005; Korkischko & Meneghini, 2010), as a way of disturbance on spanwise uniformity of vortex shedding, is the most widely used presently. Recently, triple-starting helical grooves were reported as a new method in VIV suppression and drag reduction (Huang, 2011). More information about them can be found out in reviews of Sarpkaya & Isaacson (1981), Kumar *et al.* (2008), and Wu & Sun (2009).

Meantime, another way was proposed by introducing three-dimensional geometric disturbance, such as a wavy front surface (Bearman & Owen, 1998), and totally wavy cylinders (Owen *et al.*, 1999; Lin *et al.*, 2010). However, these disturbances were introduced in a streamwise-spanwise plane and thus sensitive to the flow direction. Then a new idea that disturbance was introduced in a radial-spanwise plane, called radial disturbance, was proposed (Lin *et al.*, 2011; 2012), based on the Bernoulli equation and the effect of geometric disturbance on flow field. Initial experiments of oscillating pendulum with such disturbance in water channel have shown that such disturbance is effective in reducing oscillating amplitude at the start of lock-in, but invalid at higher reduced velocity. Due to obvious difference between pendulum and riser, it is an urgent need to investigate the physical mechanism and effect of radial disturbance on the flow around risers.

In the present paper as the basic study, the main purpose is to obtain the fundamental knowledge about the effect of radial disturbance on the flow past a circular cylinder through the numerical simulation. Two types of wavy disturbance are considered with a series of wavelength and wave steepness at a Reynolds number of 100. Firstly, the physical model is described briefly. Then effects of disturbances on fluid forces, flow patterns and generation of vorticity on cylinder surfaces are presented and analyzed, respectively. At last, conclusions are given.

## PHYSICAL MODEL

### Governing Equations

In an inertial Cartesian coordinate system  $(x,y,z)$ , an incompressible fluid flow past the circular cylinder with two types of radial disturbance, as shown in Fig. 1, is considered. The peak and valley on wavy shape are defined as spanwise positions with the maximal and minimal diameters, respectively. Then, the wavy shape can be mathematically described by the wavelength  $\lambda$  and the peak-to-valley wavy height  $W$ . The dimensionless forms of the continuity and Navier-Stokes equations are expressed as follows,

$$\nabla \cdot \mathbf{u} = 0 \quad (1)$$

$$\frac{\partial \mathbf{u}}{\partial t} + (\mathbf{u} \cdot \nabla) \mathbf{u} = -\nabla p + \frac{1}{Re} \nabla^2 \mathbf{u} \quad (2)$$

where  $\mathbf{u}$  is the velocity vector  $(u,v,w)$ ,  $p$  is the static pressure,  $Re$  is the Reynolds number defined as  $U_\infty D/\nu$  based on the free-stream velocity  $U_\infty$ , the diameter of cylinder  $D$  and the kinematic viscosity of fluid  $\nu$ , and  $\nabla$  is the gradient operator. It should be noticed that the diameter  $D$  should be selected as the minimal diameter of wavy cylinder, equal to the diameter of straight cylinder, rather than the averaged diameter. From the engineering's point of view, the disturbance as a suppression shroud is installed outside of pre-designed pipes or risers.

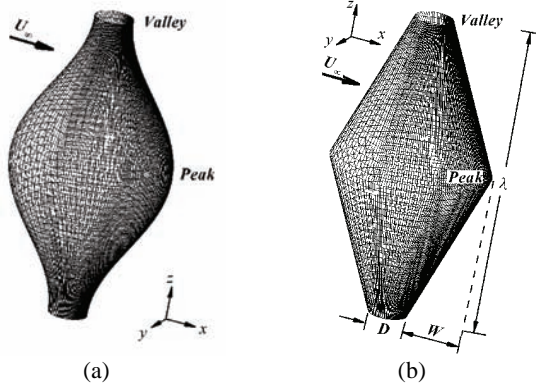


Fig. 1 Schematics of a flow past the circular cylinders with the (a) harmonic and (b) conic disturbances.

### Numerical Method

Computations are run by the Fluent software. With the assumption of the periodic flow along the span, as a method in simulating the infinite length of cylinder, boundary conditions in  $(x,y)$  plane are described as following: the uniform free-stream velocity at inlet, the non-reflecting outflow at outlet, the free slip at vertical sides and non-slip on cylinder surfaces. The non-dimensional computational domain in  $(x,y)$  plane is  $40 \times 20$ . The magnitude of convergent error for the continuity equation is less than  $10^{-3}$ .

For validation of numerical simulation, two-dimensional flow past the circular cylinder is carried out. The wake is typically described by the Kármán vortex shedding, as shown in Fig. 2. The Strouhal number,  $St$ , is 0.167. The mean drag coefficient,  $C_D$ , is 1.39, and the RMS lift coefficient,  $C_L'$ , 0.256. Through compared with previous experiments (Williamson, 1996) and numerical results (Zhan, et al., 2008), the present calculations are acceptable for further study.

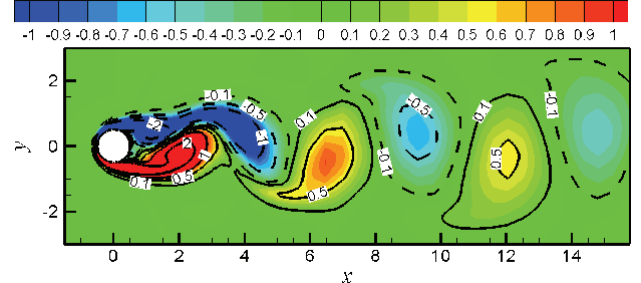


Fig. 2 Contours of spanwise vorticity in describing the Kármán vortex shedding in the near wake at  $Re=100$ .

### EFFECTS OF DISTURBANCES

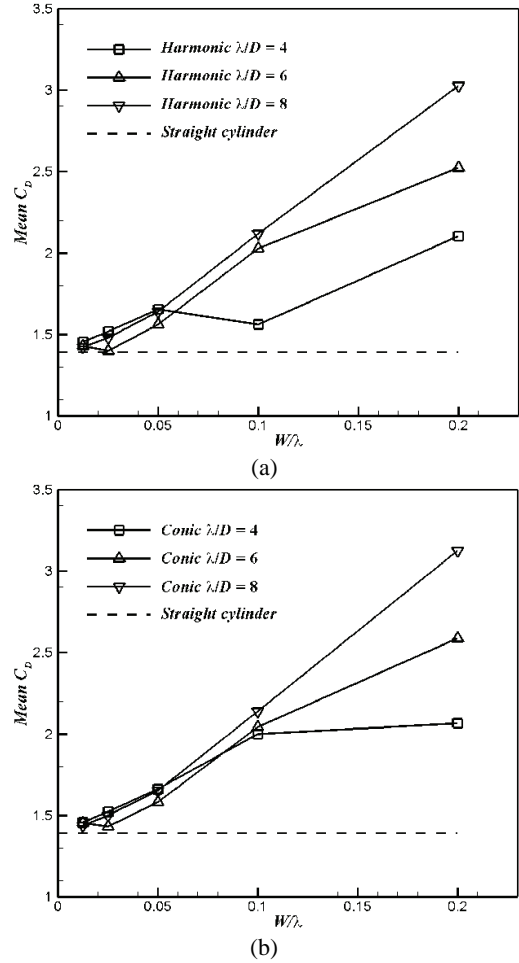


Fig. 3 Variation of the mean drag coefficient with respect to the wave steepness for the (a) harmonic and (b) conic cylinders.

In the flow past the straight cylinder, the main control parameter is the Reynolds number. As for the wavy shape, two geometric scales  $W$  and

$\lambda$  are introduced. Correspondingly, two independent length parameters are defined as the non-dimensional wavelength,  $\lambda/D$ , and wave steepness,  $W/\lambda$ . In the present study, a series of computational investigations have been carried out at the Reynolds number of 100 for different values of  $\lambda/D$  with 4, 6 and 8 and  $W/\lambda$  with 0.0125, 0.025, 0.05, 0.1 and 0.2, by reference to the previous investigation.

## Fluid Forces on Cylinders

The variations of the mean drag coefficient and the RMS lift coefficient with respect to the wave steepness are summarized in Figs. 3~4 for harmonic and conic cylinders, respectively. For the sake of convenient comparison between different cylinders, all fluid forces are normalized by the free-stream velocity and the projected area of the straight cylinder with the diameter of  $D$ . It can be seen that the overall trend of variation of drag coefficient for the harmonic cylinder is similar to that for the conic cylinder, as well as the lift coefficient.

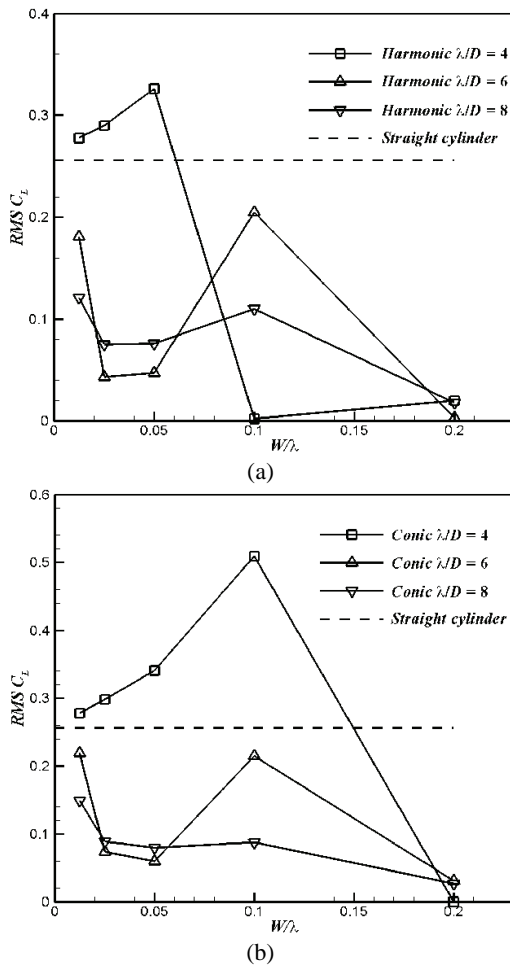


Fig. 4 Variation of the RMS lift coefficient with respect to the wave steepness for the (a) harmonic and (b) conic cylinders.

Generally, after introducing the disturbance, the drag increases with the increasing wave steepness. And the drag in all cases is greater than that of the straight cylinder. However, an interesting phenomenon is occurred at the lower wave steepness for  $\lambda/D=4$  and 6 for the harmonic cylinder, where the drag reaches a local minimum. This is also appeared in the conic cylinder for  $\lambda/D=6$ .

Different from the variation of the drag coefficient, the RMS lift

coefficient for wavy cylinders in most cases is less than that for the straight cylinder, even decreases down to zero. In present simulations, it exists mainly in cases of  $\lambda/D=6$  and 8. However, at  $\lambda/D=4$ , there is a critical value for  $W/\lambda$  where  $C'_L$  is equal to that for the straight cylinder. Only for  $W/\lambda$  greater than this critical value,  $C'_L$  is decreased. In addition, at  $W/\lambda=0.2$ ,  $C'_L$  almost reaches the lower values while  $\bar{C}_D$  reaches the maximum. Furthermore, similar phenomenon, that is the local minimum of  $C'_L$ , is also found out at the same domain of the wavelength and wave steepness, especially for  $\lambda/D=6$ . Such phenomenon can give us a hint that there exists the optimized range for specific disturbance wavelength and wave steepness with the local minimum of drag and lift forces by applying radial disturbance.

## Flow Patterns in The Near Wake

The complex variation of hydrodynamic forces shows the wake flow complicated. Therefore, different flow patterns in the near wake are classified into several regimes. The wake topology is illustrated by using the iso-surface of three components of vorticity.

### Regime I-Typical Kármán Vortex Shedding With Little Distortion.

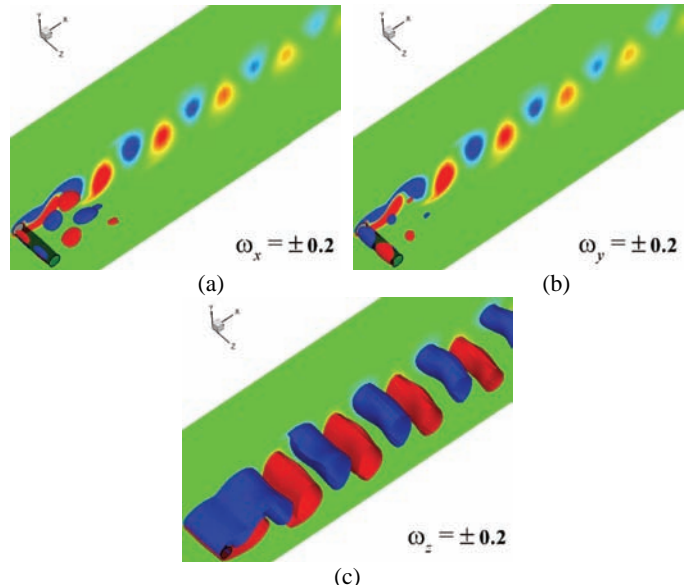


Fig. 5 Perspective views for iso-surfaces of (a)  $\omega_x$ , (b)  $\omega_y$  and (c)  $\omega_z$  in the case of the harmonic cylinder with  $\lambda/D=4$  and  $W/\lambda=0.0125$ . The positive value is red and the negative value blue. The slice at the end of cylinder is the contour of  $\omega_z$  varied from -0.5 to 0.5. The body is shown by the translucent cylinder with a black frame (same below).

Although introducing the weak disturbance, the wake dynamics is mainly characterized by the Kármán vortex alternatively shedding. It denotes the disturbance is very weak. Despite all this, the disturbance leads to the appearance of additional components of vorticity,  $\omega_x$  and  $\omega_y$ , in the near wake. They are gradually weaken and died away downstream. As a result, the pair of spanwise vortex is distorted in the near wake and transported into the far wake. In this flow pattern, the drag is gradually increased, while the lift is also increased and greater than that of straight cylinder for  $\lambda/D=4$  with the increasing wave steepness, but less for other wavelengths at  $W/\lambda=0.0125$ .

### Regime II-A-Vortex Distortion Mainly Affected By $\omega_x$ .

As for the moderate disturbance, additional components of vorticity are further increased and developed into the near wake. This results in the obvious distortion of spanwise vortex. Two types of vortex shedding are classified based on dominant effects of the streamwise vorticity and the additional vorticity. In the present flow regime, flow patterns are still described by the feature of alternative shedding of vortex.

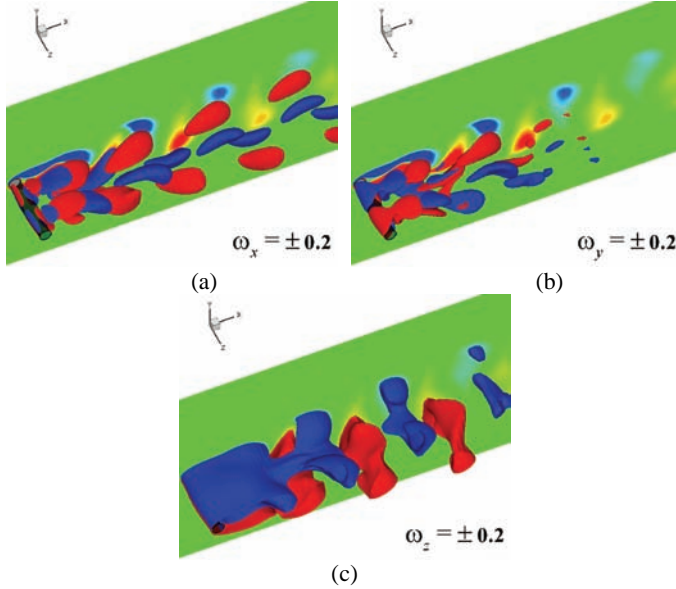


Fig. 6 Perspective views for iso-surfaces of (a)  $\omega_x$ , (b)  $\omega_y$  and (c)  $\omega_z$  in the case of the harmonic cylinder with  $\lambda/D=6$  and  $W/\lambda=0.025$ .

In the type II-A, the streamwise vorticity is developed in the near wake and further transported into the far wake. But in the far wake, the vertical vorticity is reduced quickly. As a result, the distorted direction of spanwise vortex is mainly affected by the pair of the streamwise vortex. Correspondingly, the drag and lift forces drop down to the local minimum for wavy cylinders with  $\lambda/D=6$  and  $W/\lambda=0.025$ .

#### Regime II-B-Vortex Distortion Affected By $\omega_x$ And $\omega_y$ .

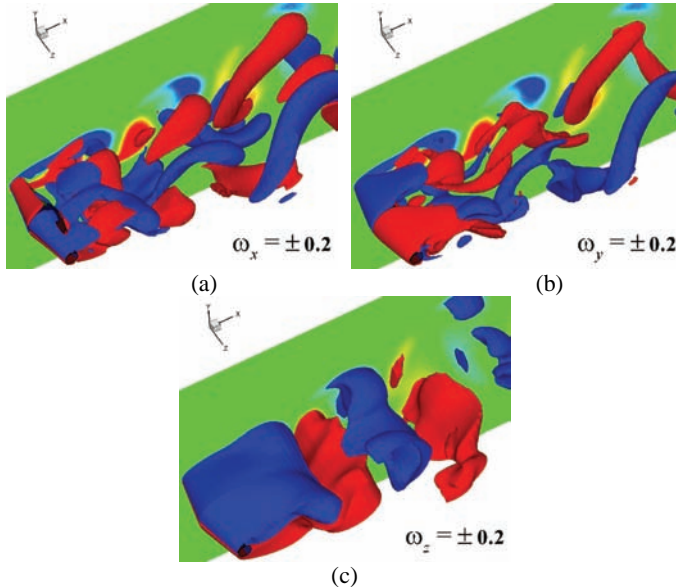


Fig. 7 Perspective views for iso-surfaces of (a)  $\omega_x$ , (b)  $\omega_y$  and (c)  $\omega_z$  in the case of the conic cylinder with  $\lambda/D=8$  and  $W/\lambda=0.1$ .

Typically as shown in Fig. 7, one of features of present flow pattern, different from that in the type II-A, is the growth of vertical vorticity far away from the body. The spanwise vortex is greatly curved by pairs of both streamwise and vertical components of vorticity. Interestingly, such vortex pattern is very similar to the mode A appeared in the flow past a square-section cylinder at the Reynolds number of 180 (Lin, 2007). The lift reaches the local maximum for  $\lambda/D=8$  and  $W/\lambda=0.01$ . And the drag is increased greatly

#### Regime III-A-Q-type Vortex At The Valley Or Peak

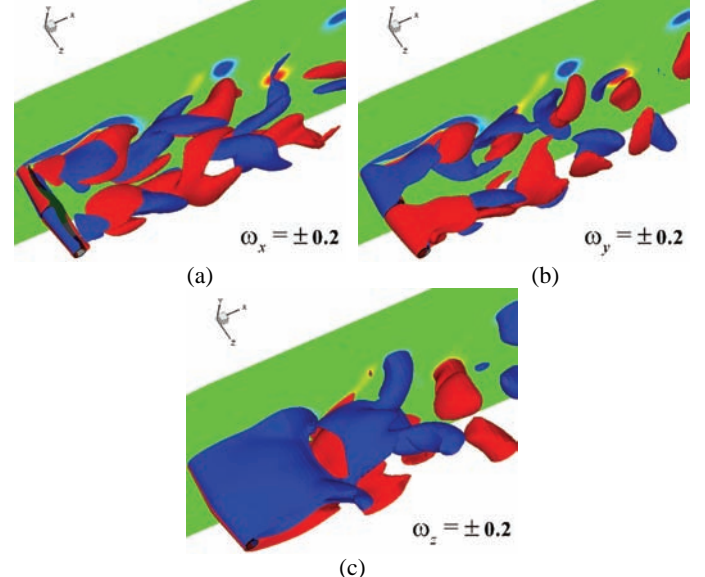


Fig. 8 Perspective views for iso-surfaces of (a)  $\omega_x$ , (b)  $\omega_y$  and (c)  $\omega_z$  in the case of the conic cylinder with  $\lambda/D=8$  and  $W/\lambda=0.05$ .

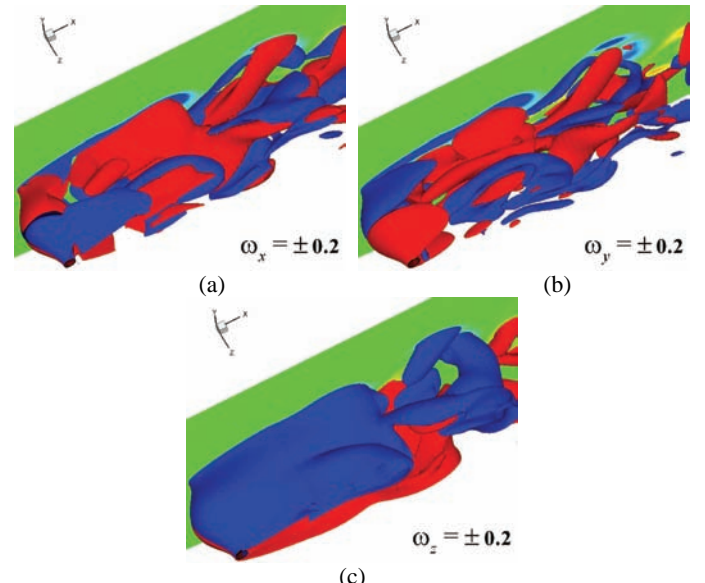


Fig. 9 Perspective views for iso-surfaces of (a)  $\omega_x$ , (b)  $\omega_y$  and (c)  $\omega_z$  in the case of the harmonic cylinder with  $\lambda/D=8$  and  $W/\lambda=0.2$ .

For strong disturbances, the main feature of the wake flow pattern is the total disappearance of Kármán vortex. Under the strong effect of streamwise and/or vertical components of vorticity, the flow becomes more and more complex. At least, three patterns are identified.

In the type III-A, with further increasing streamwise and vertical components of vorticity, the spanwise vortex is distorted violently and shed obliquely, as shown in Figs. 8~9. With the specific distribution of additional vorticity, the spanwise vortex is shed asynchronously along the span. Therefore, it seems to be bent upstream, called the  $\Omega$ -type vortex. Two kinds of vortex shedding pattern are distinguished based on the earlier shedding at the valley and peak, respectively. Another feature is that the shear layer for the  $\Omega$ -type vortex at the peak is elongated far downstream. As for the  $\Omega$ -type vortex at the valley, the lift reaches the local minimum at  $\lambda/D=8$  and  $W/\lambda=0.025$  and 0.05. Similarly, for the  $\Omega$ -type vortex at the peak, the lift is reduced down to nearly zero at  $W/\lambda=0.2$  and other wavelength.

### Regime III-B-Cloud-like Vortex

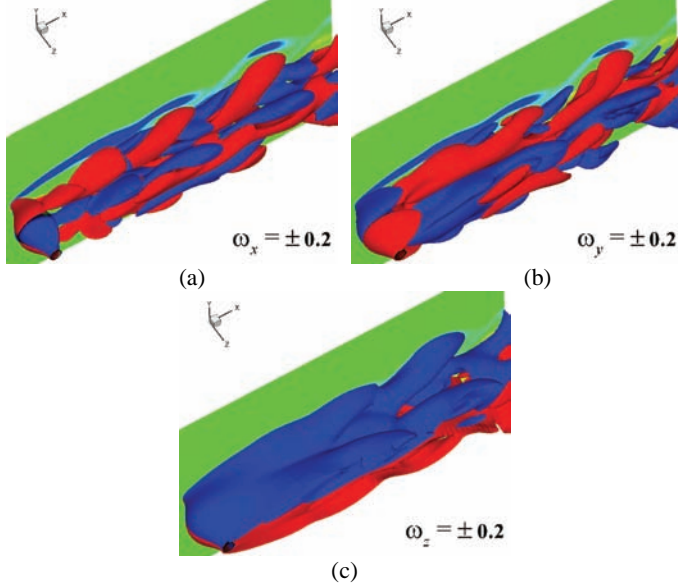


Fig. 10 Perspective views for iso-surfaces of (a)  $\omega_x$ , (b)  $\omega_y$  and (c)  $\omega_z$  in the case of the harmonic cylinder with  $\lambda/D=6$  and  $W/\lambda=0.2$ .

As typically shown in Fig. 10, two features in the type III-B are found out. The one is the shear layers reaching more far away from the body than those stated above. The other is the spanwise mainly concentrated at the valley and shed more quickly or earlier than that at the peak, which seems to be the extreme status of  $\Omega$ -type vortex shed at the valley, formed the cloud-like vortex. The unsteadiness of wake is so weak that it can be taken as a kind of means in suppressing vortex shedding. The lift is nearly zero.

### Regime III-C-Vortex Shedding Completely Suppressed

In present type, as shown in Fig. 11, there are three characteristics. The first is the streamwise vorticity obviously less than that reported in other cases with strong disturbance, and died away quickly in the near wake. The second is the vertical vorticity relatively stronger than the streamwise vorticity in the wake. The last is the total suppression of vortex shedding. Similar to the phenomenon occurred in the flow past the wavy square-section cylinder (Lin, 2010), the present physical mechanism is mainly attributed to the vertical vorticity. The flow around the wavy cylinder with certain strong disturbance leads to the strong spanwise flow behind the body. Correspondingly, the vertical vorticity on cylinder surface is generated and transported into the near wake. And the streamwise vorticity in the near wake is greatly weakened. The upper and lower shear layers are close at the peak and away at the valley each other. The physical reason is the different

distribution of streamwise velocity induced by the vertical vorticity. The interaction between shear layers is delayed effectively. From the point of view of vorticity line, the spanwise vorticity line is curved along the vertical direction and connected with the opposite one due to the strong effect of vertical vorticity. Therefore, the originally asynchronous shedding of upper and lower spanwise vortex is coordinated by such connection and gradually developed to the synchronous status. The flow is steady and symmetric about the wake center plane. The lift is zero but the drag the greatest.

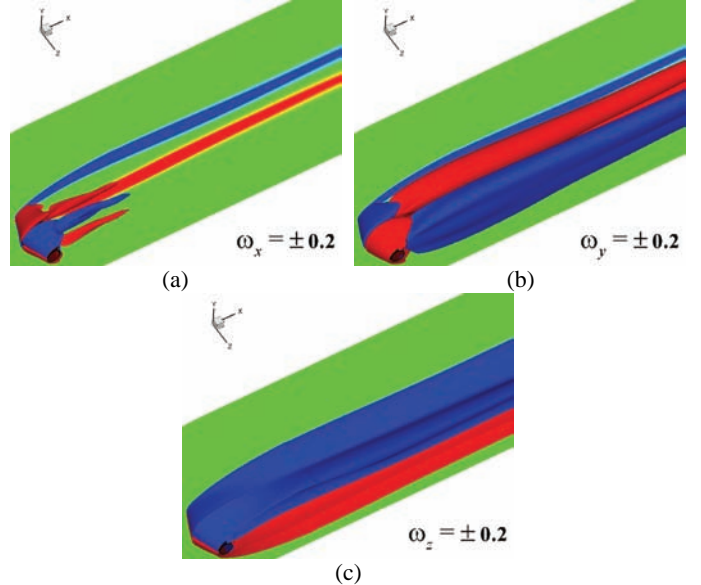


Fig. 11 Perspective views for iso-surfaces of (a)  $\omega_x$ , (b)  $\omega_y$  and (c)  $\omega_z$  in the case of the conic cylinder with  $\lambda/D=4$  and  $W/\lambda=0.2$ .

Overall, from the above analysis, different flow patterns are summarized in the following Table 1, based on the competition between the streamwise and vertical components of vorticity. It would be mentioned that there may be some new flow patterns different from above found out by carefully controlling the strength of streamwise and vertical components of vorticity at certain waviness and wavelength.

Table 1. Different flow patterns qualitatively determined by the competition between  $\omega_x$  and  $\omega_y$  in the magnitude and range, where W, M and S denote the weak, moderate and strong extent.

$\omega_x$	$\omega_y$	Regime	Physical Description of Flow Pattern
W	W	I	Kármán vortex with little distortion
M	W	II-A	Vortex shedding mainly distorted by $\omega_x$
		II-B	Vortex shedding distorted by $\omega_x$ and $\omega_y$
M	M	III-A	$\Omega$ -type vortex shedding at the valley
		III-B	$\Omega$ -type vortex shedding at the peak
S	S	III-A	$\Omega$ -type vortex shedding at the peak
		III-B	Cloud-like vortex
W	S	III-C	Vortex shedding totally suppressed

### Vorticity on Cylinder Surfaces

As we know now, vorticity is generated on cylinder surfaces due to the viscosity. Different flow patterns in the near wake are associated with the specific distribution of surface vorticity. Therefore, it is necessary to know about the effect of radial disturbance on the surface vorticity.

At the Reynolds number of 100, the wake flow past the straight cylinder is characterized by two-dimensional Kármán vortex shedding. Correspondingly, only  $\omega_z$  is generated on cylinder surfaces and invariant along the spanwise direction.

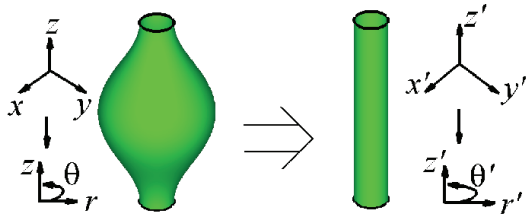


Fig. 12 Schematic diagram of transformation from the original cylindrical coordinates to the new cylindrical coordinates by using a mapping of Eq. 3. The wavy cylinder is then stretched along the radial direction to be a straight cylinder.

For the sake of convenience, the analysis is carried out in the cylindrical coordinates due to the circular sections for commonly used risers. The original cylindrical coordinate system,  $(r, \theta, z)$ , is established for the fixed wavy cylinder, as shown in Fig. 12. The wavy shape along the span is described by a function of geometric disturbance,  $\xi(z)$ . By introducing a mapping transformation, the wavy cylinder is stretched to be a straight cylinder in the radial direction. The mapping, originated from the idea proposed by Newman (1996), is defined by

$$r' = r + \xi(z), \quad \theta' = \theta, \quad z' = z \quad (3)$$

where  $(r', \theta', z')$  is a new cylindrical coordinate system, or called the transformed coordinate system. It should be noticed that there are three assumptions, no twist along the span, small waviness with amplitudes less than 1, and all spanwise sections parallel to each other. As a result, the velocity vector is transformed as follow,

$$V'_r = V_r + V_z \xi'(z), \quad V'_\theta = V_\theta, \quad V'_z = V_z \quad (4)$$

where the additional velocity,  $V_z \xi'$ , is appeared in the radial velocity due to the mapping transformation, and  $\xi'$  is the function of wave steepness,

$$\xi'(z) = \frac{d\xi}{dz} = \frac{d\xi}{dz'} \quad (5)$$

Similarly, relationships of spatial derivatives between the original and transformed coordinates are obtained,

$$\frac{\partial}{\partial r} = \frac{\partial}{\partial r'}, \quad \frac{\partial}{\partial \theta} = \frac{\partial}{\partial \theta'}, \quad \frac{\partial}{\partial z} = \frac{\partial}{\partial z'} + \frac{d\xi}{dz'} \frac{\partial}{\partial r'} \quad (6)$$

Three components of vorticity in the original coordinate system are expressed by

$$\omega_r = \frac{1}{r} \frac{\partial V_z}{\partial \theta} - \frac{\partial V_\theta}{\partial z} \quad (7)$$

$$\omega_\theta = \frac{\partial V_r}{\partial z} - \frac{\partial V_z}{\partial r} \quad (8)$$

$$\omega_z = \frac{1}{r} \frac{\partial(rV_\theta)}{\partial r} - \frac{1}{r} \frac{\partial V_r}{\partial \theta} \quad (9)$$

With consideration of the non-slip condition on cylinder surfaces and transformation between two coordinate systems, the relationships of surface vorticity are obtained,

$$\omega_r|_{r'=\frac{D}{2}} = \omega'_r|_{r'=\frac{D}{2}} - \frac{d\xi}{dz'} \frac{\partial V_\theta'}{\partial r'}|_{r'=\frac{D}{2}} \quad (10)$$

$$\omega_\theta|_{r'=\frac{D}{2}} = \omega'_\theta|_{r'=\frac{D}{2}} - \left( \frac{d\xi}{dz'} \right)^2 \frac{\partial V_z'}{\partial r'}|_{r'=\frac{D}{2}} \quad (11)$$

$$\omega_z|_{r'=\frac{D}{2}} = \omega'_z|_{r'=\frac{D}{2}} \quad (12)$$

where the vorticity on the stretched straight cylinder, as well as that on the real straight cylinder just in expressions, is given by

$$\omega'_r|_{r'=\frac{D}{2}} \equiv 0 \quad (13)$$

$$\omega'_\theta|_{r'=\frac{D}{2}} = - \frac{\partial V_z'}{\partial r'}|_{r'=\frac{D}{2}} \quad (14)$$

$$\omega'_z|_{r'=\frac{D}{2}} = \frac{\partial V_\theta'}{\partial r'}|_{r'=\frac{D}{2}} \quad (15)$$

Therefore, the new relationships of vorticity on the wavy cylinder with circular sections are obtained as following,

$$\omega_r|_{r'=\frac{D}{2}} = - \frac{d\xi}{dz'} \omega_z|_{r'=\frac{D}{2}} \quad (16)$$

$$\omega_\theta|_{r'=\frac{D}{2}} = - \left[ 1 + \left( \frac{d\xi}{dz} \right)^2 \right] \frac{\partial V_z'}{\partial r'}|_{r'=\frac{D}{2}} \quad (17)$$

By comparing surface vorticity between straight and wavy cylinders, Eqs. 13~17, three features are identified as the result of radial disturbance. The first is the generation of radial and tangential components of vorticity on the wavy cylinder. Among of them,  $V_r$  is never appeared on the straight cylinder. But  $V_\theta$  can be generated on the straight cylinder due to the three-dimensional instability. The second is  $V_r$  linearly proportional to the wave slope and the spanwise vorticity, as a direct result of disturbance. Its specific distribution could be predicted qualitatively based on the selected wavy shape and distribution of spanwise vorticity, as well as its quantitative estimation. The last is the tangential component non-linearly proportional to the wave slope and increased with the increase of spanwise flow near the body, which seems that the tangential vorticity is an indirect effect of disturbance.

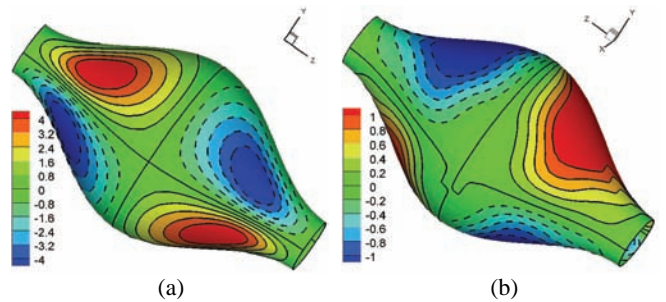


Fig. 13 Contours of the streamwise vorticity on (a) front and (b) rear surfaces in the case of harmonic cylinder with  $\lambda/D=6$  and  $W/\lambda=0.2$ .

Such features would help us to understand the physical mechanism of disturbance in generation of additional components of surface vorticity in Cartesian coordinate system. In the Cartesian system, two

characteristics of additional vorticity can also be analyzed similarly based on above relationships and computations, typically as shown in Figs. 13~14. The first is the direction of streamwise component varied alternatively along the spanwise and tangential directions on surfaces. But the direction of vertical component on surfaces is just varied along the span because it is mainly determined by the tangential component or spanwise velocity. The second is the magnitude of vorticity on the front surface obviously greater than that on the rear surface. As a result, the development of additional components of front surface vorticity mainly disturbs the shear layers shed from the front surface, as shown in Figs. 7~11. Whilst, the transport of additional vorticity on the rear surface makes the flow behind the body complicated.

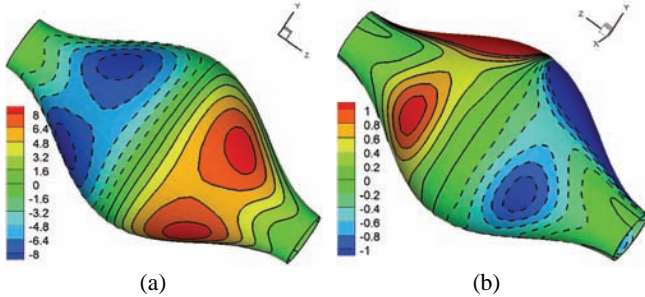


Fig. 14 Contours of the vertical vorticity on (a) front and (b) rear surfaces in the case of harmonic cylinder with  $\lambda/D=6$  and  $W/\lambda=0.2$ .

## CONCLUSIONS

Numerical simulations are carried out to investigating effects of radial disturbance on flows past the circular-section cylinder. Two kinds of disturbance are harmonic and conic. Non-dimensional wavelength, 4, 6 and 8, and wave steepness, 0.0125, 0.025, 0.05, 0.1 and 0.2, are considered. The Reynolds number is 100.

The introduction of disturbance results in the drag increasing almost linearly as the increase of wave steepness, which is greater than that for the straight cylinder. However, the lift is reduced for most cases, except for the wavelength of 4, by comparison to that for the straight cylinder, even down to near zero. Interestingly, there is a region where the fluid forces reach the local minimum. This gives us a hope in applying such disturbance, like for an optimized design.

At the Reynolds number of 100, the successively increasing disturbance results in the original Kármán vortex gradually disturbed. Due to the generation and development of additional components of vorticity, the flow pattern becomes more and more complex. Several different regimes in differentiating characteristics of these patterns are identified qualitatively. For example, the Kármán vortex is kept at the weak disturbance. At for the moderate disturbance, the spanwise vortex is still shed alternatively, but distorted by the increase of streamwise and vertical components of vorticity. When such disturbance becomes strong,  $\Omega$ -type vortex, cloud-like vortex, and the complete suppression of vortex shedding are distinguished at different wave steepness.

Through analysis of vorticity on cylinder surfaces in the cylindrical coordinate system, relationships between three components of surface vorticity and disturbance are obtained. The radial component is linearly proportional to the wave steepness, while the tangential one is non-linearly varied. Similarly, the feature of additional vorticity in the Cartesian system is similar to that in the cylindrical system.

## ACKNOWLEDGEMENTS

The authors sincerely acknowledge the support of the National Key Scientific Instrument and Equipment Development Program of China (No. 2011YQ120048) for the work reported in this paper.

## REFERENCES

- Bearman, PW, and Owen, JC (1998). "Reduction of bluff-body drag and suppression of vortex shedding by the introduction of wavy separation lines," *J Fluids Struct*, Vol 12, pp 123-130.
- Gabbai, RD, and Benaroya, H (2005). "An overview of modeling and experiments of vortex-induced vibration of circular cylinders," *J Sound Vib*, Vol 282, pp 575-616.
- Huang, S (2011). "VIV suppression of a two-degree-of-freedom circular cylinder and drag reduction of a fixed circular cylinder by the use of helical grooves," *J Fluids Struct*, Vol 27, pp 1124-1133.
- Korkischko, I, and Meneghini, JR (2010). "Experimental investigation of flow-induced vibration on isolated and tandem circular cylinders fitted with strakes," *J Fluids Struct*, Vol 26, pp 611-625.
- Kumar, RA, Sohn, CH, and Gowda, BHL (2008). "Passive control of vortex-induced vibrations: an overview," *Recent Patents on Mechanical Eng*, Vol 1, No 1, pp 1-11.
- Lee, L, and Allen, DW (2005). "The dynamic stability of short fairings," *Offshore Tech Conf Houston*, Texas, USA, OTC 17125.
- Lin, LM (2007). "Wake dynamics and forces in the flow around the square-section cylinder with a geometric disturbance," PhD thesis, Institute of Mechanics, Chinese Academy of Sciences.
- Lin, LM, Ling, GC, and Wu, YX (2010). "Mechanism responsible for the complete suppression of Karman vortex in flows past a wavy square-section cylinder," *Chin Phys Lett*, Vol 27, No 3, pp 034702.
- Lin, LM, Zhong, XF, and Wu YX (2011). "Experimental investigation of a new device in suppressing vortex-induced vibrations of a circular cylinder," *Proc 21st Int Offshore and Polar Eng Conf*, Maui, Hawaii, ISOPE, Vol 3, pp 1283-1288.
- Lin, LM, Zhong, XF, and Wu YX (2012). "Vortex-induced vibrations of a circular cylinder with different geometric disturbances," *Proc 22nd Int Offshore and Polar Eng Conf*, Rhodes, Greece, ISOPE, Vol 3, pp 623-629.
- Newman, DJ (1996). "A computational study of fluid/structure interactions: flow-induced vibrations of a flexible cable," PhD thesis, Princeton University, pp 9-13.
- Owen, JC, Szewczyk, AA, and Bearman, PW (1999). "Suppressing Kármán vortex shedding by use of sinuous circular cylinders," *Bulletin of the American Physical Society*, Vol 44, pp 124.
- Owen, JC, Bearman, PW, and Szewczyk, AA (2001). "Passive control of VIV with drag reduction," *J Fluids Struct*, Vol 15, pp 597-605.
- Sarpkaya, T (1979). "Vortex-Induced Oscillations—A Selective Review," *J Appl Mech*, Vol 46, pp 241-258.
- Sarpkaya, T (2004). "A critical review of the intrinsic nature of vortex-induced vibrations," *J Fluids Struct*, Vol 19, pp 389-447.
- Sarpkaya, T, and Isaacson, M (1981). *Mechanics of wave forces on offshore structures*. Van Nostrand Reinhold Company, 606pp.
- Song, JN, et al. (2009). "Experimental investigation of suppression of vortex-induced vibration of marine risers by three control rods," *Ocean Eng*, Vol 27, No 3, pp 23-29.
- Trim, AD, Braaten, H, Lie, H, and Tognarelli, MA (2005). "Experimental investigation of vortex-induced vibration of long marine risers," *J Fluid Struct*, Vol 21, pp 335-361.
- Williamson, CHK (1996). "Vortex dynamics in the cylinder wake," *Annu. Rev. Fluid. Mech.* Vol 28, pp 477-539.
- Williamson, CHK, and Govardhan, R (2004). "Vortex-induced vibrations," *Annu Rev Fluid Mech*, Vol 36, pp 413-455.
- Wu, H, and Sun, DP (2009). "Study on suppression measures for vortex-induced vibration of the deepwater riser," *China Offshore Platform*, Vol 24, pp 1-8.

Zhan, H, et al. (2008). "Numerical simulation of the flow around a circular cylinder at varies Reynolds number," J. WuHan Univ. Tech. Vol 30, pp 129-132.